Volume 149
Number 4
21 February 2024
Pages 977-1338

Analyst

rsc.li/analyst

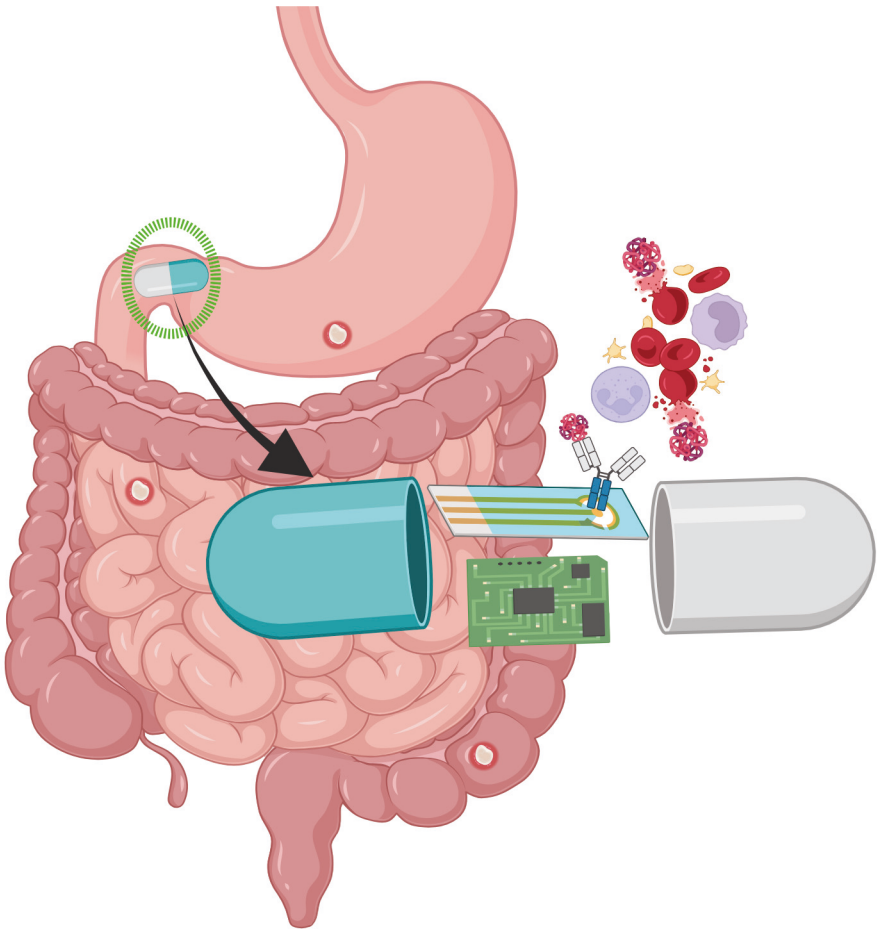

ISSN 0003-2654

ROYAL SOCIETY OF CHEMISTRY

PAPER
Ata Khalid *et al.*
A low-cost miniature immunosensor for haemoglobin as a device for the future detection of gastrointestinal bleeding

Analyst

ROYAL SOCIETY OF CHEMISTRY

PAPER

View Article Online
View Journal | View Issue

Check for updates

Cite this: *Analyst*, 2024, **149**, 1081

A low-cost miniature immunosensor for haemoglobin as a device for the future detection of gastrointestinal bleeding†

Alper Demirhan,[a] Iva Chianella,[b] Samadhan B. Patil[c,d] and Ata Khalid *[a]

Gastrointestinal bleeding (GIB) is a serious medical condition, which requires immediate attention to establish the cause of the bleeding. Here, we present the development of a miniaturised electrochemical impedance spectroscopy (EIS) device for the detection of GIB. The device performs EIS measurements up to 100 kHz. Following the development of an immunosensor for haemoglobin (Hb) on screen printed electrodes, the EIS device was used for detecting Hb as an early indication of bleeding. The sensor was able to detect Hb in a redox solution in a linear range between 5 μg mL^{-1} and 60 μg mL^{-1}, with a limit of detection of 13.3 μg mL^{-1}. It was also possible to detect Hb in simulated intestinal fluid, without the need for a redox solution, within a range of 10 μg mL^{-1} to 10 mg mL^{-1} with a limit of detection of 2.31 mg mL^{-1}. The miniature EIS device developed in this work is inexpensive, with an estimated cost per unit of £30, and has shown a comparable performance to existing commercial tools, demonstrating its potential to be used in the future as an ingestible sensor to detect GIB. All these measurements were carried out in a purpose built flow cell with supporting hardware electronics outside the cell. Integration of the hardware and the sensing electrodes was demonstrated in pill form. This pill after integration sampling fluidics has potential to be used in detecting gastrointestinal bleeding.

Received 12th December 2023,
Accepted 15th December 2023

DOI: 10.1039/d3an02147e

rsc.li/analyst

Open Access Article. Published on 11 January 2024. Downloaded on 3/13/2024 9:21:35 AM.
This article is licensed under a Creative Commons Attribution 3.0 Unported Licence.

Introduction

Gastrointestinal bleeding (GIB) is a serious condition that refers to bleeds occurring in the gastrointestinal tract from the mouth to the rectum. The most common reasons for GIB are peptic ulcers, erosive diseases, and varices. Death usually occurs for patients whose bleeding is recurring or not stopping.[1] The latter happens in 25% of diagnosed cases, and those patients are at a high risk of mortality.[2] GIB is classified as upper GIB (UGIB) or lower GIB (LGIB) depending on whether the location is above or below the ligament of Treitz. Around 80% of GIB is UGIB of which an estimated 60% is caused by peptic ulcers.[3] The mortality rate caused by GIB is around 5–10%.[4]

Despite advanced diagnosis and treatment technologies, the mortality rate related to GIB is still high. Diagnosis and treatment of GIB are expensive and represent a serious economic burden since they involve a high level of hospital resources.[5] The cost of treatment and mortality rate would be significantly lowered if there were a device or technique capable of detecting traces of blood in the minutest amount at an early stage of GIB. The technique or device should be inexpensive and minimally invasive. However, since the GI tract is about 9 m in length, diagnosis is challenging. The most common diagnostic methods include endoscopy, colonoscopy, CT, surgery, and immunochemical testing. In general, endoscopy is used to identify the bleeding location and investigate other symptoms in the UGI tract, while colonoscopy is used to investigate the LGI tract. Sometimes faecal occult blood tests can be used for detection of bleeds in faeces by immunochemistry.[6] However, since haemoglobin degrades when travelling long distances in the GI tract, such tests can detect a limited number of cases and only when the source of bleeding is in the LGI tract. Although endoscopy is the first-line choice for the diagnosis of GIB, its missing rate for bleeding is 10% if the lesions are in the area accessible using an endoscope; otherwise it goes up to 18%.[2] Also, endoscopy needs to be performed by skilled nurses or doctors and requires hospital admission. Recently, video capsule endoscopy (VCE) has been

[a]*Center for Electronic Warfare, Information and Cyber, Cranfield University, Defence Academy of the UK, Shrivenham SN6 8LA, UK.*
E-mail: ata.khalid@cranfield.ac.uk
[b]*Surface Engineering and Precision Centre, School of Aerospace, Transport and Manufacturing, Cranfield University, Bedford MK43 0AL, UK*
[c]*School of Physics, Engineering and Technology, University of York, York YO10 5DD, UK*
[d]*York Biomedical Research Institute (YBRI), University of York, York YO10 5DD, UK*
† Electronic supplementary information (ESI) available. See DOI: https://doi.org/10.1039/d3an02147e

Open Access Article. Published on 11 January 2024. Downloaded on 3/13/2024 9:21:35 AM.
This article is licensed under a Creative Commons Attribution 3.0 Unported Licence.

used for the diagnosis of GIB.[7] VCE uses a pill sized swallowable device, and it consists of a camera, LEDs, a signal processor, a battery, and an antenna. While it travels through the body, a camera records a video of the GI tract and transmits the video wirelessly to a recorder. However, VCE does not fully meet all medical needs; it is expensive, consumes a lot of power, and requires expert interpretation of hours of video. Swallowable non-white light optical capsules have been used instead of VCE for the detection of GIB.[8–12] These capsules use fluorescence[9] or illuminance[12] instead of digital cameras. Hence, they require no complex software and consume less power compared to VCE. Nonetheless, these capsules require complicated instruments. There are also associated safety issues, as optical capsules may require injection of fluorescein dye (or programmed bacteria) into the human body to develop and capture an illuminance signal as a result of their interaction with haemoglobin.

Among other studies, Yen *et al.* (2017)[13] have suggested an ingestible haemoglobin immunosensor using a gallium arsenide based molecular controlled semiconductor resistor device. They have detected haemoglobin between 10 μg mL^{-1} and 100 μg mL^{-1} in fasted-state simulated intestinal fluid (FASSIF). The limit-of-detection was 1.13 μg mL^{-1}. Nevertheless, the apparatus was designed for endoscopy rather than as a stand-alone capsule. McCaffrey *et al.*[14] have designed electrochemical sensors as swallowable capsules for investigation of the gastrointestinal tract. Although the capsule incorporated potentiostat circuitry, it was not able to perform electrochemical impedance spectroscopy (EIS) but could perform other voltammetric techniques such as cyclic and square wave voltammetry. The capsule was designed to work as an electronic tongue to enable the non-specific characterisation of gut fluids in the small intestine, aiding the diagnosis of conditions such as Crohn's disease and ulcerative colitis.

EIS is a label-free and non-destructive method which measures the surface impedance of electrodes caused by changes occurring on the sensor surface such as by antibody–antigen binding. The change in impedance is evaluated to assess the presence and concentration of target molecules. The impedance is usually calculated by applying an AC voltage and measuring the corresponding current. Then, the ratio of voltage and current is used to calculate the impedance. Although there are several devices for EIS, they are unsuitable for use as ingestible devices since they are bulky, expensive, and power hungry (ESI S1 and Table S1†). Nonetheless, devices for EIS can be developed into inexpensive devices that are small enough to be incorporated in a swallowable pill.

Therefore, here, we present a novel and miniaturised EIS device, which was then used as an immunosensor for the detection and quantification of haemoglobin to establish an early signature of GIB. The instrument includes an analog lock-in amplifier (LIA) synchronised with a direct-digital synthesiser (DDS) to achieve high performance, while being low-cost and small-size (Fig. 1A and B). Its cost was estimated to be around £30 (Table S2†). Since haemoglobin is an abundant protein in blood with unique chemical characteristics, we chose it as the model protein to indicate the presence of bleeding. The performance of the instrument was compared with that of a commercial device by measuring haemoglobin in a redox buffer (Fig. 1C and D). A schematic illustration depicting the working principle of our device in the GI environment is presented in Fig. 1E. Finally, we demonstrated the detection of haemoglobin in FASSIF using our device and the flow-cell without the use of a redox probe to mimic the GI environment (Fig. 1F). The size of the instrument was kept at 33 × 20 mm^2 for practical reasons, but it can be easily scaled to smaller sizes as shown in Fig. 1G and H.

Experimental design

Instrument architecture

The developed instrument consists of inexpensive, low-power, and off-the-shelf components. We used a DDS to generate waveforms with a high-sampling rate in an optimised way without using complicated hardware and software. An analog LIA was designed to down-convert AC signals to DC using analog switches instead of a high-speed, power-hungry analog-to-digital converter (ADC). Then the demodulated signal was digitised with a 24-bit ADC. Since most of the work was done with individual analog circuits, less work was required in the digital domain. Hence, for the microcontroller unit (MCU), we used EFM8LB12 (Silicon Labs, USA), which is an 8-bit, 8051-core MCU, with an internal clock up to 72 MHz, a 4× 12-bit digital-to-analog converter (DAC), and several timer modules within a small package (4 × 4 mm^2). Thus, we have achieved a high-performance instrument without using power hungry components, such as field-programmable gate arrays (FPGA). This architecture also opens up a way to obtain optimised application specific integrated circuit (ASIC) designs for EIS based sensors since performing analog computation can be more power and area efficient.[15] The sensor's current was converted to voltage with a transimpedance amplifier (TIA). The gain of the TIA was controlled with a tiny digital potentiometer instead of using a network of analog switches as in most other works.[16,17] Inaccuracies caused by the TIA gain and op-amps were calibrated with dummy cells. Thus, highly accurate (<0.5% gain error and <1° phase error) measurements in frequencies up to 100 kHz were achieved (Table S3†).

Experiments were conducted with the instrument shown in Fig. 1B. Nonetheless, after removing unnecessary parts such as the USB connector, and dividing the single board into two smaller pieces that can be stacked on top of each other for further miniaturisation, the same instrument was able to fit into a capsule as shown in Fig. 1G and H. These further simplifications did not affect the sensor's performance as the overall electronic architecture remained the same. The capsule included two 1.55 V coin-cells, two printed-circuit boards (PCB), and one electrode. The electrode was a screen-printed electrode trimmed to fit into the capsule, or it could be thin-film electrodes[18] since these two types of electrodes are similar.

This journal is © The Royal Society of Chemistry 2024

Open Access Article. Published on 11 January 2024. Downloaded on 3/13/2024 9:21:35 AM.
This article is licensed under a Creative Commons Attribution 3.0 Unported Licence.

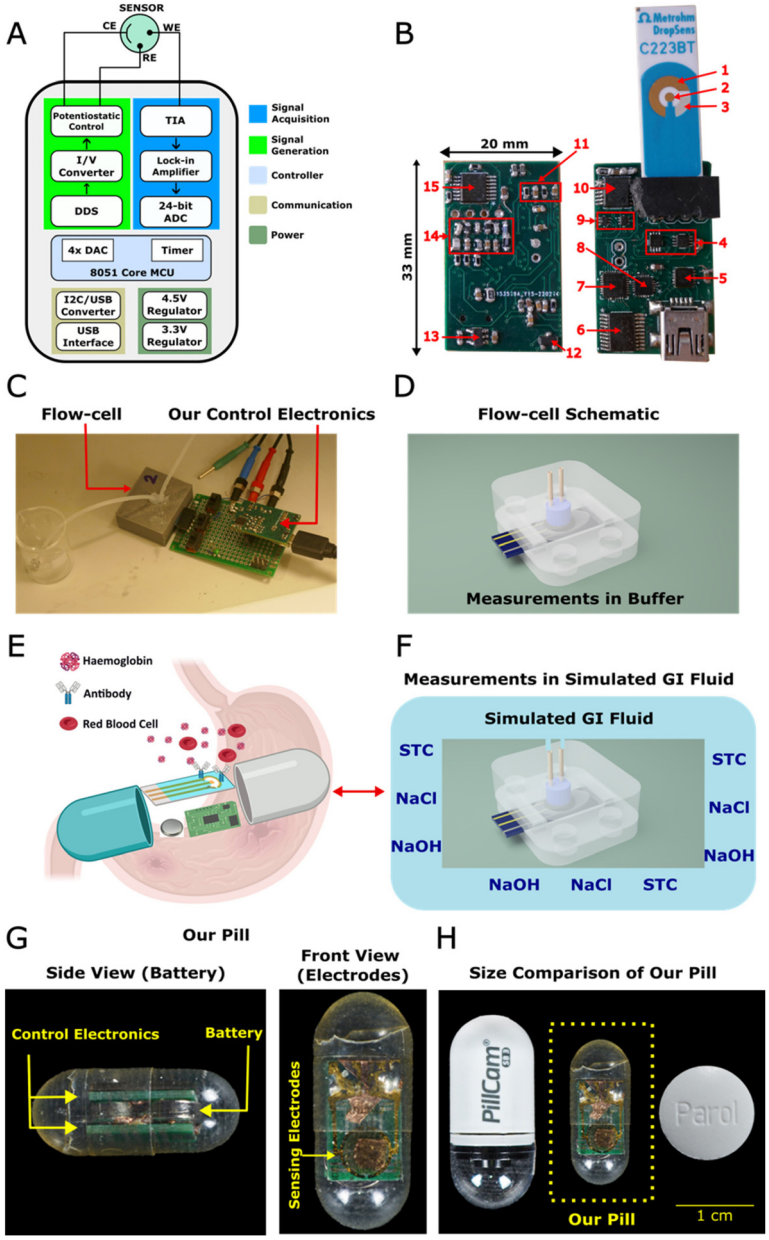

Fig. 1 (A) Architecture of the instrument. I2C: inter-integrated circuit; DAC: digital-to-analog converter; MCU: microcontroller unit; DDS: direct-digital synthesiser; CE: counter electrode; RE: reference electrode; WE: working electrode; TIA: transimpedance amplifier; ADC: analog-to-digital converter. (B) Bottom and front face of the instrument. 1: RE; 2: WE; 3: CE; 4: 2× MAX5394 (digital potentiometers); 5: FT200XD (I2C/USB converter); 6: AD9834 (DDS); 7: EFM8LB12 (MCU); 8: MCP3561 (ADC); 9: 2x PI5A3157 (analog switch); 10: OPA4354 (op-amp); 11: low-pass filter for the lock-in amplifier; 12: MCP1700 (3.3 V regulator); 13: LP2985 (4.5 V regulator); 14: 7^{th} order low-pass filter; 15: OPA4354 (op-amp). (C) Experimental setup. (D) Schematic of the flow-cell. (E) Illustration of working principle of the proposed pill (Created by biorender.com). (F) Flow-cell in simulated GI fluid environment. (G) Our pill which is a smaller version of B after removing unnecessary parts such as USB. (H) Size comparison of our pill with PillCam and paracetamol.

Signal generation

There are many methods reported in the literature for signal generation, but to implement LIA, the frequency of the generated signal and LIA must be exactly matched. Because of this, digitally controlled signal generation methods are often preferred. DDS is a method to produce arbitrary waveforms by using digital calculations. It can be implemented either by a DAC and a controller[19] or by off-the-shelf integrated circuits (ICs).[20] Since DDS ICs include optimised building blocks to produce sinusoidal waveforms, they do not have any software complexity, and they consume lower power compared to custom made DDS. Hence, we used AD9834 (Analog Devices, USA), which is a current-output DDS IC used for generation of sine waves. The output frequency of DDS was determined using $f_{MCLK} \times W/2^{28}$, where f_{MCLK} is the clock input to DDS,

Open Access Article. Published on 11 January 2024. Downloaded on 3/13/2024 9:21:35 AM.
This article is licensed under a Creative Commons Attribution 3.0 Unported Licence.

which was provided by the timer module of the microcontroller, and W is the value of a 28-bit frequency register which is user-programmable. The value of f_{MCLK} is up to 75 MHz, which means it can generate signals as low as 0.27 Hz and can be tuned to 0.004 Hz resolution. The full-scale amplitude of the output current was adjusted by the current flowing through the full-scale adjustment (FSA) pin of DDS. Hence, to control the full-scale amplitude, a 10 kΩ resistor was connected between a DAC and the FSA pin.

Signal acquisition

The current flowing through the working electrode (WE) was converted to voltage by an OPA4354 (Texas Instruments, USA) operational amplifier (op-amp) working in TIA configuration. Gain of the TIA was adjusted using a MAX5394 (Maxim Integrated, USA), which is an 8-bit, 100 kΩ digital potentiometer (Fig S1†). Although its −3 dB bandwidth was 1600 kHz and 165 kHz for 10 kΩ and 100 kΩ, respectively, its response was calibrated. DC current flowing through the sensor can cause saturation of the TIA before amplifying the AC current. Hence, before each measurement, an opposing DC current was applied to null the DC current of the sensor.

Lock-in amplifier

A lock-in amplifier, sometimes known as a synchronous demodulator or an I/Q (in-phase/quadrature) demodulator, is used to measure very small signals. It can be implemented by analog or digital methods. Nonetheless using digital LIA requires high speed ADC, memory, and controllers such as FPGA, which increase the cost and power consumption.[21] For this reason, a square-wave based lock-in amplifier was designed to demodulate AC signals to the DC level. This design is also easier to scale for a higher number of channels compared to digital LIA, since it is cheaper, smaller, and simpler. To filter harmonic frequencies properly, the signal was averaged by measuring it for 1 second for frequencies higher than 100 Hz and averaged for at least 2 seconds for lower frequencies. The MCP3561 (Analog Devices, USA) is a 24-bit differential input ADC, and it was used to measure the differential output voltage of the LIA. It also has a programmable gain amplifier, which can amplify the output signal up to 16 times. This helped us to increase the sensitivity and dynamic range of the measurements.

Calibration of the instrument

The calibration of the instrument was the key point to get maximum performance with low-cost and small size components. By measuring inaccuracies in the circuit, it was possible to account for them by re-calculating the results. We measured and calibrated the circuit elements in 6 steps (Fig. S2†). Finally, inaccuracies, phase shifts and offsets caused by the circuit elements were calibrated using reference resistors. The instrument measured the impedance spectrum of 4 reference resistors. These measured values were stored in a MATLAB script. After each V_{sensor} measurement, the MATLAB script was used to calculate the corresponding Z_{sensor} value using $(V_{reference} - V_{offset}) \times Z_{reference}/(V_{sensor} - V_{offset})$, where V_{offset} is the voltage when the electrodes were open-circuited, and $V_{reference}$ is the voltage obtained from reference resistor measurements.

Chemical sensing of haemoglobin

Chemicals. Phosphate buffered saline tablets (PBS, pH 7.4), isopropanol, potassium ferricyanide $[K_3Fe(CN)_6]$, potassium ferrocyanide $[K_4Fe(CN)_6]$, bovine serum albumin (BSA), and purified human haemoglobin were purchased from Sigma Aldrich (Dorset, UK). Human anti-haemoglobin antibodies were purchased from Fisher Scientific (UK). Antibodies were aliquoted and stored at −20 °C. FASSIF powder and FASSIF buffer were purchased from Biorelevant (London, UK). All chemicals were of analytical reagent grade.

Apparatus. Electrochemical measurements for the antibody optimisation experiments were conducted using a Palmsens-4 (Palmsens, The Netherlands). Haemoglobin measurements using the redox solution were performed by both Palmsens-4 and the proposed device. FASSIF experiments were performed only with the device developed in this work. Dropsens C223-BT screen-printed electrodes (SPE) were purchased from Metrohm (Runcorn, UK). Working and counter electrodes were gold, whereas the reference electrode was silver. A flow-cell was used to simulate the testing environment (Fig. 1D and F). Solutions were injected with a syringe. Mechanical switches were used to select the device connected to the electrode.

Fabrication of the immunosensor. The immunosensor was developed by immobilising anti-haemoglobin antibodies onto the SPE surface *via* physical adsorption (Fig. 2). For this, electrodes were first washed by dipping them in isopropanol for 10 minutes, followed by immersion in DI water for another 10 minutes. Antibody solutions prepared in PBS were dispensed on the SPE to cover all the electrode areas and these were incubated in the fridge overnight at +4 °C. The following

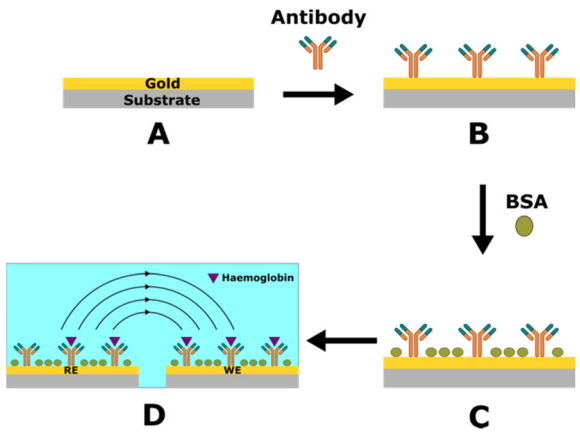

Fig. 2 Development of the immunosensor. (A) Bare metal electrodes were cleaned by washing with isopropanol. (B) Antibodies in PBS were dropped on electrodes and incubated overnight at +4 °C. (C) Bovine serum albumin (BSA) was used to block empty spaces on the surface. (D) EIS measurements were carried out in a flow-cell.

This journal is © The Royal Society of Chemistry 2024

Open Access Article. Published on 11 January 2024. Downloaded on 3/13/2024 9:21:35 AM.
This article is licensed under a Creative Commons Attribution 3.0 Unported Licence.

day, the electrodes were washed with plenty of PBS. Afterwards, to block the electrode surface, 1% (w/v) BSA solution was dropped onto the electrodes and incubated for one hour. Then, the SPE was washed with plenty of PBS to remove unbound molecules.

Haemoglobin measurement in redox solution. An AC potential with 10 mV_{RMS} was applied to keep the sensor's response in a linear range. The open-circuit potential was measured before each experiment, and the equilibrated value was applied as DC bias to sensor. The frequency range was set between 5 Hz and 50 kHz in 41 steps (10 frequencies per decade). There was an interval of 10 seconds before each EIS measurement to allow the sensor to reach its steady state and prevent transient response. Measurements were performed firstly with Palmsens-4, and right after they were repeated with our device using the same parameters.

For the measurements, firstly, PBS solution was dropped onto electrodes and incubated for 20 minutes. Then, the impedance spectrum of the sensor was measured in 5 mM $K_4Fe(CN)_6/K_3Fe(CN)_6$ solution prepared in PBS (pH 7.4). This impedance spectrum was considered the baseline response (R_{CT_0}). Afterwards, electrodes were washed with PBS and incubated for 20 minutes with a solution of haemoglobin prepared in PBS. Then the sensor's impedance spectrum was measured again (R_{CT_HGB}). A new SPE was used for each haemoglobin concentration. All measurements were fitted with the Randles circuit. Changes of the R_{CT} value before and after haemoglobin measurement were used to calculate the correlation between haemoglobin concentration and the impedance spectrum using the following equation:

$$R_{CT}(\%) = \frac{R_{CT_HGB} - R_{CT_0}}{R_{CT_0}} \times 100 \quad (1)$$

Haemoglobin measurement in simulated intestinal fluid (FASSIF). Since redox solutions give a non-linear response, a small amplitude perturbation (10 mV_{RMS} for this work) was needed.[23] However, as FASSIF is not a redox solution, we first tested the linearity of the sensor in FASSIF by measuring its impedance at different AC potentials. Then, an AC potential of 50 mV was applied to the sensor to get a higher signal-to-noise ratio without disturbing the environment. A frequency range between 10 Hz and 100 kHz in 41 steps (10 frequencies per decade) was used for the measurements. The DC voltage was fixed at 0 V. An equilibrating period of 10 seconds was used before each experiment to allow the sensor to reach its steady state and prevent a transient response. FASSIF was prepared by mixing 10.41 g of FASSIF buffer with 240.3 g of DI water. Then, 0.560 g of FASSIF powder was added to the solution. After the solution was mixed thoroughly with a magnetic stirrer until full dissolution, it was left to stand for 2 hours for stabilisation. The sensor was prepared as explained in the previous section. After the antibody immobilisation and blocking with BSA, the impedance spectrum of the electrode was measured in FASSIF (Z_{blank}). Then, haemoglobin concentrations prepared in FASSIF were incubated for 20 minutes, and after the electrodes were washed with FASSIF buffer, the EIS measurement was performed in the buffer, (Z_{HGB}). Since FASSIF measurements are non-faradaic (in the absence of a redox probe), impedance at 12.59 Hz (rather than R_{CT}) was considered for calculations. The impedance change was calculated using the following equation:

$$\Delta Z(\%) = \frac{Z_{HGB} - Z_{blank}}{Z_{blank}} \times 100 \quad (2)$$

Results and discussion

System validation and comparison of the performance

To test the accuracy and precision of the device, measurements were carried out with a dummy cell in the frequency range from 1 Hz to 100 kHz and the response was compared with that of Palmsens-4. Reference and counter electrodes were short-circuited and a 10 mV_{RMS} signal was applied. A complex dummy cell was used to measure the performance of both devices in the presence of a capacitive load (Fig. 3A). The results show that the performance of our device is comparable to that of Palmsens-4 and the mean amplitude errors recorded were 105.42 Ω and 85.41 Ω, for our device and Palmsens-4, respectively. The plot in Fig. 3A also shows that our instrument can properly differentiate imaginary and real parts in the whole range of the spectrum. An accuracy plot was generated by measuring resistors between 40 Ω and 51 kΩ (Fig. 3B and Table S4†). We observed that at lower impedances (<10 kΩ)

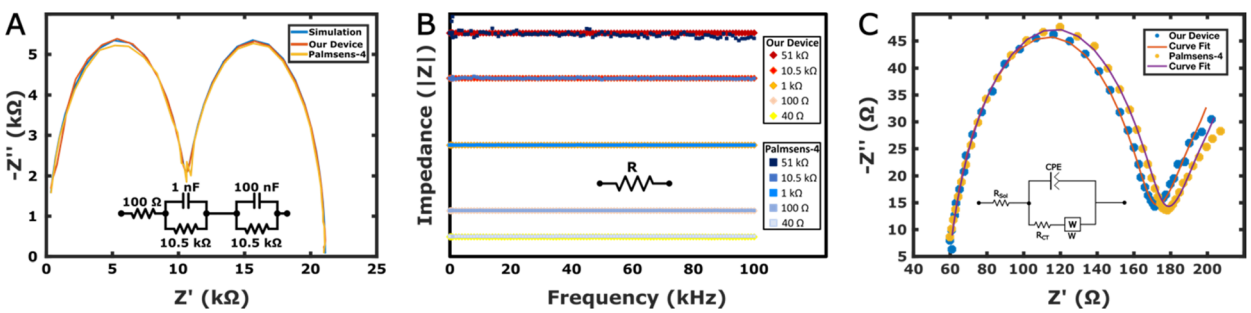

Fig. 3 (A) Dummy cell measurement with both devices. (B) Accuracy contour plot between 1 Hz and 100 kHz. The *y*-axis is logarithmic. (C) Measurement of the redox buffer with unmodified electrodes.

Open Access Article. Published on 11 January 2024. Downloaded on 3/13/2024 9:21:35 AM.
This article is licensed under a Creative Commons Attribution 3.0 Unported Licence.

both the devices performed similarly. Error and standard deviation were less than 1%. Nonetheless, at higher impedances, our device performed better. For example, the commercial device (Palmsens-4) measured a 51 kΩ reference resistor with 11.47% standard deviation whereas our device measured it with 0.12% standard deviation. Considering that the real device would work in the physiological environment (GI fluid medium) inside the body, this is an important point to note since GI fluid exhibits low conductivity as demonstrated by the simulated intestinal fluid (FASSIF) experiments. We also observed that the accuracy plot is flat and does not show any low-pass filter characteristics at the impedance and frequency range of interest; hence, it will enable accurate measurements.

Electrode characterisation

Electrode characterisation was performed by cyclic voltammetry (CV) and EIS in 5 mM $K_4Fe(CN)_6/K_3Fe(CN)_6$ solution. CV experiments were performed at different scan rates, and linear relationships between the peak current and scan rate were found with R^2 = 0.99 for both devices (Fig. S3†). Similarly, when EIS measurements of a bare electrode were also performed with both devices, the results were comparable and both showed characteristics of a Randles equivalent circuit (Fig. 3C and Table S4†).

Electrode modification steps

The impedance spectrum of the SPE was measured after each modification. There was an increase in impedance after each step, as shown in Fig. S4 and Table S5.† This was due to the sensor's surface being covered with additional non-conductive layers (antibodies and proteins), which block the electrode–electrolyte interface.

Antibody immobilisation optimisation

Anti-haemoglobin antibody in several concentrations (25, 50, 100, and 200 μg mL^{-1}) was prepared in PBS buffer. The binding of 10 μg mL^{-1} haemoglobin was evaluated to find the antibody concentration generating the maximum response. The best response was obtained when the antibody's concentration used for the immobilisation on the electrodes was 100 μg mL^{-1} (Fig. S5†). Therefore, this concentration was used in all the subsequent experiments. The higher antibody concentration (200 μg mL^{-1}) resulted in a lower signal for haemoglobin, indicating the presence of steric hindrance caused by the antibody being immobilised too tightly on the sensor surface.

Calibration curve in redox solution

Calibration curves were obtained by measuring haemoglobin concentrations between 5 and 60 μg mL^{-1} with both our device and Palmsens-4, by recording the signal in the same redox solution (5 mM $K_4Fe(CN)_6/K_3Fe(CN)_6$). The Randles equivalent circuit shown in the inset of Fig. 3C was used to fit the data and the charge transfer resistance (R_{ct}) was used to evaluate impedance changes. The Python module impedance.py was used for circuit fitting for both devices.[22]The calibration curves in the range between 5 μg mL^{-1} and 60 μg mL^{-1} are shown in Fig. 4C and D for both devices. The relationships between the impedance change and the haemoglobin concentration were $\Delta R_{CT}(\%)$ = 1.48 [Haemoglobin] (μg mL^{-1}) + 19.61 and $\Delta R_{CT}(\%)$ = 1.61 [Haemoglobin] (μg mL^{-1}) + 16.47 for our

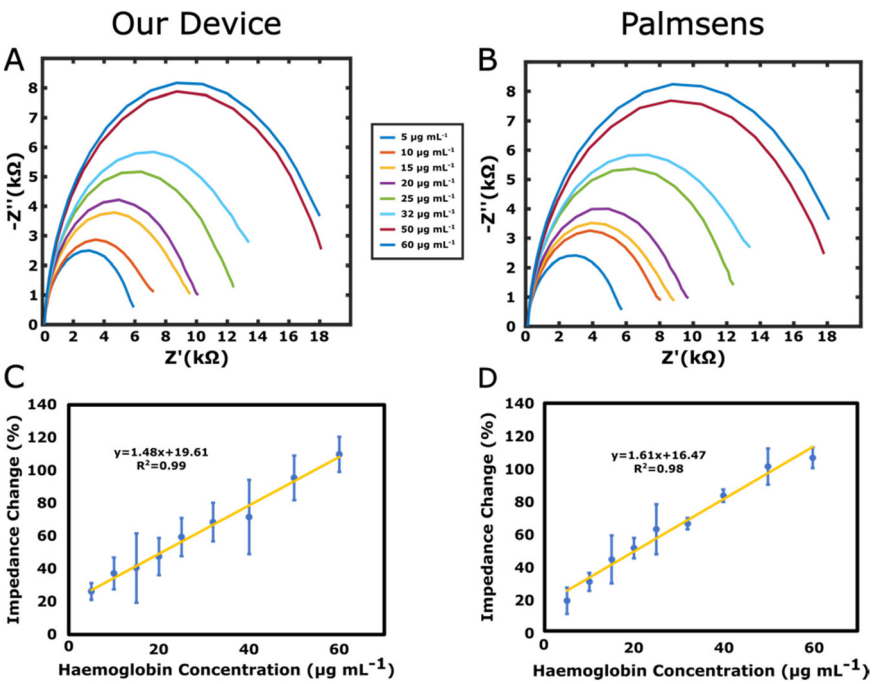

Fig. 4 Haemoglobin measurements in redox solution. (A) and (B) Raw data of the impedance spectrum for our device and Palmsens-4, respectively. (C) and (D) Calibration curve of haemoglobin concentration measurement with our device and Palmsens-4, respectively.

This journal is © The Royal Society of Chemistry 2024

Open Access Article. Published on 11 January 2024. Downloaded on 3/13/2024 9:21:35 AM.
This article is licensed under a Creative Commons Attribution 3.0 Unported Licence.

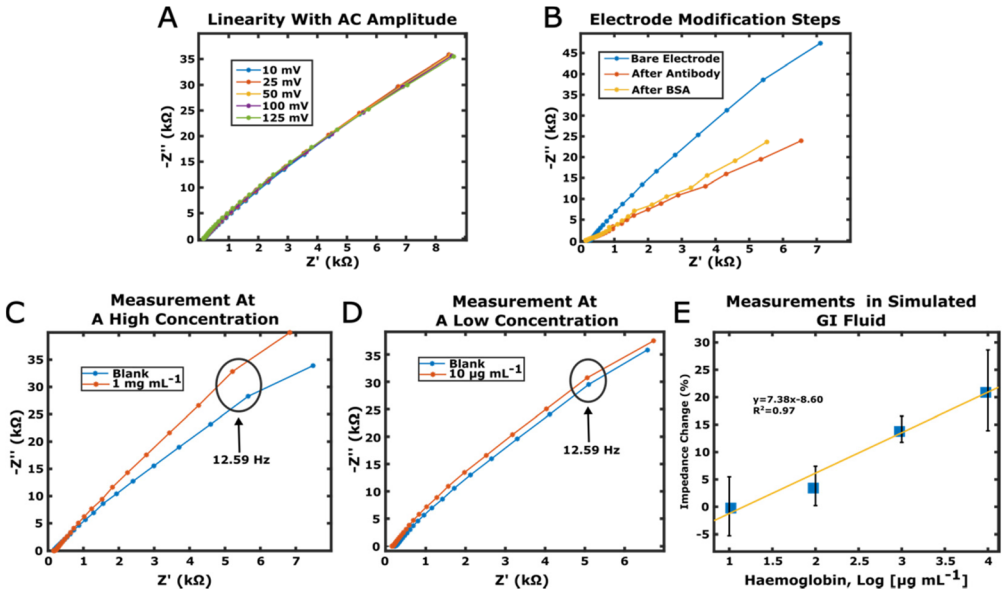

Fig. 5 Haemoglobin measurements in FASSIF. (A) EIS response of bare electrode for different AC voltages. (B) Impedance response of the sensor after antibody and BSA immobilisation. (C and D) Sensor's response to 1 mg mL^{-1} and 10 µg mL^{-1} of haemoglobin in FASSIF. Circled value corresponds to 12.59 Hz. (E) Calibration curve of haemoglobin in FASSIF.

device and Palmsens-4, respectively. The R^2 values were 0.99 and 0.98 for our device and Palmsens-4, respectively. The limits of detection (LOD) calculated as the averaged blank readings + 3× standard deviation were found to be 13.3 µg mL^{-1} and 16.1 µg mL^{-1} for our device and Palmsens-4, respectively.[24] The error bars shown in Fig. 4C and D are often relatively high. One of the reasons for this is that the measurements were performed across the two devices subsequently. Each measurement was first conducted with the Palmsens followed by our device. However, when switching between devices, while adjusting the cables, the electrodes were sometimes unintentionally biased with wrong DC voltages, as the feedback loop was temporarily broken. Hence, due to this, at times, the open circuit potential value was changed accidentally before the measurements, contributing to larger errors. To mitigate this problem, further experiments should be conducted with only one device with minimal intervention to the experimental setup.

To check the specificity of the immunosensor, we measured the concentration of haemoglobin in the absence of the antibody, when only the blocking agent was present on the sensor surface. The corresponding result, displayed in Fig. S6† shows that without the antibodies, no significant change in impedance was observed while increasing the concentration of haemoglobin, demonstrating both the presence of a low degree of non-specific binding to the sensor surface and the specificity of the antibody–haemoglobin reaction.

Calibration curve in simulated intestinal fluids (FASSIF)

A calibration curve was obtained by measuring increasing haemoglobin concentrations between 10 µg mL^{-1} and 10 mg mL^{-1} prepared in simulated intestinal fluid (FASSIF). Only our device was used for FASSIF experiments. In addition, as the measurements were carried out in the absence of the $K_4Fe(CN)_6/K_3Fe(CN)_6$ redox probe (non-faradaic EIS), rather than fitting the spectra to an equivalent circuit, the impedance values recorded at 12.59 Hz were used. This was because, as explained in a study conducted by Shoute and colleagues,[25] the correlation between the concentration of the analyte in solution and the impedance can provide a better analytical signal at this frequency. At higher frequencies, the capacitance of the sensor became short-circuited, making it impossible to measure any meaningful impedance change.

Firstly, the linearity of the spectrum was tested by applying different AC voltages, with the bare electrode immersed in FASSIF. The spectra appeared to be the same when the AC voltage was between 10 mV and 125 mV (Fig. 5A). Therefore, an AC voltage of 50 mV was selected for the measurement, as this value represents a good compromise between a sensitive sensor signal and minimal interferences from the environment. The impedance spectra obtained after each step of the immunosensor preparation are shown in Fig. 5B.

Examples of differences in the impedance at 12.59 Hz between the signal for the blank (no haemoglobin) and two different concentrations of haemoglobin are reported in Fig. 5C and D, while the whole calibration curve in FASSIF is depicted in Fig. 5E. The relationship between the impedance change and the haemoglobin concentration was found to be $\Delta Z(\%) = 7.38 \log[\text{Haemoglobin (µg mL}^{-1})] - 8.60$, with a value of R^2 of 0.97. The LOD was calculated as 2.3 mg mL^{-1}.

Conclusions

In this work, we have developed a miniaturised and inexpensive EIS instrument specifically designed for use in

Open Access Article. Published on 11 January 2024. Downloaded on 3/13/2024 9:21:35 AM.
This article is licensed under a Creative Commons Attribution 3.0 Unported Licence.

ingestible devices for detection of GIB. The developed device includes a direct-digital synthesiser and an analog lock-in amplifier with off-the-shelf components to facilitate miniaturisation. To assess its performance, we conducted a comparative analysis between our device and a commercial counterpart. We measured the haemoglobin concentration using both devices while performing EIS readings in a redox solution ($K_4Fe(CN)_6$/$K_3Fe(CN)_6$ solution) and obtained comparable results. In addition, our device effectively detected haemoglobin not only when using the redox solution, but also when EIS readings were carried out directly in a simulated intestinal fluid.

With an estimated cost of £30 and potential for further downsizing, our device holds great potential as an affordable and efficient point-of-care screening of GIB, which could help in reducing mortality rates and clinical costs. Besides, the sensor proposed here is a label-free, simple device that does not require skilled personnel for its use, and might, therefore, be a promising alternative to endoscopic methods for the detection of GIB. In the future, communication protocols such as intrabody communication or Bluetooth[26] can be implemented for data transfer between the pill and the outside of the body. Also, aptamers can be used instead of antibodies for more durable and stabile operations inside the body.[27] As soon as our device provided a positive signal, the patient could be admitted to hospital for further investigations with standard laboratory-based analysis, enabling diagnosis of GIB quickly and at a very early stage, reducing mortality and overall health costs. The affordability as well as the high performance would make the device proposed in this work an excellent over the counter product, representing the first screening tool for GIB.

Conflicts of interest

A. D. is a founder of Sensitify Biotechnology (Ankara, Turkey) which manufactures potentiostats. The other authors declare that they have no known competing financial interests or personal relationships that could appear to influence the work reported in this paper.

Acknowledgements

A. D. would like to thank the Ministry of National Education of Turkey for providing a doctoral scholarship.

References

1 A. J. Stanley and L. Laine, *Br. Med. J.*, 2019, 364.
2 E. W. Lee and J. M. Laberge, *Tech. Vasc. Interv. Radiol.*, 2004, **7**, 112–122.
3 J. Barnert and H. Messmann, *Nat. Rev. Gastroenterol. Hepatol.*, 2009, **6**, 637–646.
4 B. S. M. Kim, B. T. Li, A. Engel, J. S. Samra, S. Clarke, I. D. Norton and A. E. Li, *World J. Gastrointest. Pathophysiol.*, 2014, **5**, 467–478.
5 A. Viviane and B. N. Alan, *Value Health*, 2008, **11**, 1–3.
6 G. Soraya, T. Nguyen, C. Abeyrathne, D. Huynh, J. Chan, P. Nguyen, B. Nasr, G. Chana, P. Kwan and E. Skafidas, *Biosensors*, 2017, **7**, 19.
7 D. Miley, L. B. Machado, C. Condo, A. E. Jergens, K.-J. Yoon and S. Pandey, *Adv. Devices Instrum.*, 2021, **2021**, 1–30.
8 M. Ryou, A. Nemiroski, D. Azagury, S. N. Shaikh, M. B. Ryan, R. M. Westervelt and C. C. Thompson, *Gastrointest. Endosc.*, 2011, **74**, 189–194.
9 A. Nemiroski, M. Ryou, C. C. Thompson and R. M. Westervelt, *Lab Chip*, 2015, **15**, 4479–4487.
10 Z. He, L. Zhou, B. Luo, B. Hu, X. Du and Y. Li, in *Optics and Photonics for Information Processing VIII*, ed. A. A. S. Awwal, K. M. Iftekharuddin, M. A. Matin and A. Márquez, SPIE, 2014, vol. 9216, p. 921606.
11 M. W. Alam, S. S. Vedaei and K. A. Wahid, *Cancers*, 2020, **12**, 890.
12 M. Mimee, P. Nadeau, A. Hayward, S. Carim, S. Flanagan, L. Jerger, J. Collins, S. McDonnell, R. Swartwout, R. J. Citorik, V. Bulović, R. Langer, G. Traverso, A. P. Chandrakasan and T. K. Lu, *Science*, 2018, **360**, 915–918.
13 Y. K. Yen, E. Capua and R. Naaman, *IEEE Sens. J.*, 2017, **17**, 660–666.
14 C. Mc Caffrey, K. Twomey and V. I. Ogurtsov, *Sens. Actuators, B*, 2015, **218**, 8–15.
15 M. Judy, N. C. Poore, P. Liu, T. Yang, C. Britton, D. S. Bolme, A. K. Mikkilineni and J. Holleman, *IEEE. Trans. Circuits Syst. I: Regul. Pap.*, 2018, **65**, 2764–2773.
16 T. Piasecki, K. Chabowski and K. Nitsch, *Measurement*, 2016, **91**, 155–161.
17 D. M. Jenkins, B. E. Lee, S. Jun, J. Reyes-De-Corcuera and E. S. McLamore, *J. Electrochem. Soc.*, 2019, **166**, B3056–B3065.
18 E. Saygili, B. Orakci, M. Koprulu, A. Demirhan, E. Ilhan-Ayisigi, Y. Kilic and O. Yesil-Celiktas, *Anal. Biochem.*, 2020, **591**, 113538.
19 M. Carminati, A. Rottigni, D. Alagna, G. Ferrari and M. Sampietro, 2012 IEEE I2MTC – International Instrumentation and Measurement Technology Conference, Proceedings, 2012, pp. 264–267.
20 R. Salahandish, F. Haghayegh, G. Ayala-Charca, J. E. Hyun, M. Khalghollah, A. Zare, B. Far, B. M. Berenger, Y. D. Niu, E. Ghafar-Zadeh and A. Sanati-Nezhad, *Biosens. Bioelectron.*, 2022, **203**, 114018.
21 K. Kishore and S. A. Akbar, *IEEE Sens. J.*, 2020, **20**, 10345–10354.
22 M. D. Murbach, B. Gerwe, N. Dawson-Elli and L. Tsui, *J. Open Source Softw.*, 2020, **5**, 2349.
23 S. Wang, J. Zhang, O. Gharbi, V. Vivier, M. Gao and M. E. Orazem, *Nat. Rev. Methods Primers*, 2021, **1**, 1–21.
24 J. N. Miller and J. C. Miller, *Statistics and chemometrics for analytical chemistry*, Pearson/Prentice Hall, 2005.

 This journal is © The Royal Society of Chemistry 2024

25 L. C. T. Shoute, G. N. Abdelrasoul, Y. Ma, P. A. Duarte, C. Edwards, R. Zhuo, J. Zeng, Y. Feng, C. L. Charlton, J. N. Kanji, S. Babiuk and J. Chen, *Microsyst. Nanoeng.*, 2023, **9**, 1–16.
26 C. Cheng, Y. Wu, X. Li, Z. An, Y. Lu, F. Zhang, B. Su and Q. Liu, *Sens. Actuators, B*, 2021, **349**, 130781.
27 A. Teniou, A. Rhouati, S. Rabai, G. Catanante and J.-L. Marty, *Analyst*, 2023, **148**, 3899–3908.

Open Access Article. Published on 11 January 2024. Downloaded on 3/13/2024 9:21:35 AM.
This article is licensed under a Creative Commons Attribution 3.0 Unported Licence.

https://dspace.org/

A low-cost miniature immunosensor for haemoglobin as a device for the future detection of gastrointestinal bleeding

Demirhan, Alper; Chianella, Iva; Patil, Samadhan B.; Khalid, Ata

2024-02-21
Royal Society of Chemistry (RSC)
https://doi.org/10.1039/d3an02147e
Demirhan A, Chianella I, Patil SB, Khalid A. (2024) A low-cost miniature immunosensor for haemoglobin as a device for the future detection of gastrointestinal bleeding. Analyst. Volume 149, Issue 4, February 2024, pp. 1081-1089

Downloaded from a DSpace repository. https://dspace.org/